Diagn Interv Radiol 2026; DOI: 10.4274/dir.2025.253555

MODALITY-BASED (US, CT, MRI, PET-CT) IMAGING

ORIGINAL ARTICLE

Automated calculation of slice-specific volume computed tomography dose index, water-equivalent diameter, and size-specific dose estimation for computed tomography scans

Supawitoo Sookpeng[1]
Rosario Lopez-Gonzalez[2]
Suwapim Chanlaor[3]
Boriphat Kadman[1]

[1]Naresuan University, Faculty of Allied Health Sciences, Department of Radiological Technology, Phitsanulok, Thailand

[2]University of Glasgow, Institute of Neurosciences and Psychology, Department of Clinical Physics and Bioengineering, Glasgow, United Kingdom

[3]Buddhachinaraj Phitsanulok Hospital, Department of Radiology, Phitsanulok, Thailand

Corresponding author: Supawitoo Sookpeng

E-mail: supawitoos@nu.ac.th

Received 18 July 2025; revision requested 01 September 2025; last revision received 05 October 2025; accepted 13 October 2025.

Epub: 03.11.2025

Publication date: 04.05.2026

DOI: 10.4274/dir.2025.253555

PURPOSE

To develop and validate an automated computational tool for calculating a slice-specific volume computed tomography (CT) dose index ($CTDI_{vol}$), a water-equivalent diameter (D_w), and size-specific dose estimates (SSDEs) from CT images, addressing limitations of conventional console-displayed values that provide only averaged values across scan regions.

METHODS

A custom ImageJ macro was developed based on methodologies proposed in American Association of Physicists in Medicine reports 220 and 293. The tool employs threshold-based body contour segmentation [−140 Hounsfield unit (HU)] to extract patient cross-sectional areas and calculates slice-specific D_w using mean CT numbers. Slice-specific $CTDI_{vol}$ values are estimated by normalizing scanner-displayed $CTDI_{vol}$ to individual slice exposure values from Digital Imaging and Communications in Medicine metadata. An SSDE was computed using appropriate correction factors for head and body examinations. Validation was performed using water phantoms, anthropomorphic phantoms, and clinical datasets from ≥30 patients. Two Siemens CT scanners were evaluated: SOMATOM go.Top®, with console-displayed values, and SOMATOM Force®, with Radimetrics software. Agreement was assessed using intraclass correlation coefficients (ICCs) and Bland–Altman analysis.

RESULTS

Water phantom validation demonstrated excellent accuracy, with differences of <2.3% for both D_w and SSDEs. The macro required approximately 30 seconds per examination to complete the analysis. Bland–Altman plots confirmed clinically acceptable mean differences. Importantly, the slice-specific approach revealed substantial intra-scan dose variations not captured by console-reported averages, particularly in the chest phantom, where SSDEs ranged from 5.77 to 23.68 mGy despite identical average values. For the clinical dataset, ICC (3,1) values for Scanner A indicated good to excellent agreement across both head and chest/abdomen examinations (head CT—$CTDI_{vol}$: 0.974, D_w: 0.893, SSDE: 0.965; chest/abdomen CT—$CTDI_{vol}$: 1.000, D_w: 0.994, SSDE: 0.989). By contrast, Scanner B demonstrated near-perfect agreement for head CT in $CTDI_{vol}$ (0.996) and SSDE (0.967) but poor agreement for D_w (0.267). For chest/abdomen CT, however, Scanner B showed consistently high agreement, with ICC values ranging from 0.884 to 1.000.

CONCLUSION

The developed ImageJ macro provides accurate, transparent, and low-cost open-source solution slice-specific CT dose estimation that correlates well with commercial systems while offering superior spatial resolution. This automated method overcomes the limitations of traditional dose reporting by providing detailed slice-by-slice dose variations, which are often overlooked in average summary values, allowing for more accurate and clinically meaningful dose assessments.

CLINICAL SIGNIFICANCE

This tool supports detailed dose evaluation across scan regions, helping optimize protocols and enhance radiation safety. Its slice-specific approach is especially useful in anatomically complex areas and research, offering clinicians more precise dose information to guide patient care.

KEYWORDS

Size-specific dose estimate, water-equivalent diameter, volume computed tomography dose index, ImageJ, dose calculation, patient-specific dosimetry

You may cite this article as: Sookpeng S, Lopez-Gonzalez R, Chanlaor S, Kadman B. Automated calculation of slice-specific volume computed tomography dose index, water-equivalent diameter, and size-specific dose estimation for computed tomography scans. *Diagn Interv Radiol*. 2026;32(3):342-350.

Computed tomography (CT) examinations contribute substantially to radiation exposure in the general population due to their relatively high radiation doses. Radiation doses to individual organs are associated with both deterministic effects, such as skin burns and epilation, and stochastic risks, including cancer induction and genetic mutations.[1-3] Accurate quantification of the radiation dose received by a patient undergoing a CT scan is essential for both radiation protection and clinical optimization. Traditionally, the CT radiation dose has been reported using the volume CT dose index ($CTDI_{vol}$) and the dose-length product (DLP), both of which are derived from output measurements in 16- and 32-cm cylindrical polymethyl methacrylate phantoms. However, $CTDI_{vol}$ is primarily dependent on exposure parameters (e.g., tube current and tube voltage) and does not account for patient size.[4-6] Given that larger patients receive relatively low radiation doses for the same $CTDI_{vol}$, size correction methods have been proposed to improve dose estimation accuracy.

To address the limitations of $CTDI_{vol}$, the American Association of Physicists in Medicine (AAPM) introduced the size-specific dose estimate (SSDE) in Report 204.[7] The SSDE adjusts $CTDI_{vol}$ based on patient size, providing a more individualized dose estimate at the center of the scanned region. The patient's physical dimensions, derived from CT images, are used in SSDE calculations. Initially, AAPM Report 204 relied on geometric size as a proxy for X-ray attenuation. However, since X-ray attenuation depends on tissue density and composition, different anatomical regions (e.g., thorax vs. abdomen) exhibit varying attenuation properties, even when their geometric sizes are identical. For instance, the thorax, being less dense than the abdomen, results in higher radiation exposure for the same $CTDI_{vol}$. To further refine SSDE calculations, AAPM Report 220[8] introduced the concept of the water-equivalent diameter (D_w), which represents the diameter of a cylindrical water volume with equivalent mean attenuation. This approach accounts for tissue composition and provides a more accurate, patient-specific dose estimation; D_w is derived from attenuation values in axial images along the z-axis. More recently, AAPM Report 293 extended the application of SSDEs to head CT examinations by incorporating region-specific correction factors.[9]

Several studies have suggested that SSDEs serve as a more reliable surrogate for organ-absorbed doses on a slice-by-slice basis.[10-12] In clinical practice, automatic tube current modulation (ATCM) is widely implemented in CT imaging, adjusting the tube current according to the attenuation level in the xy-plane and along the z-axis. Consequently, $CTDI_{vol}$ and SSDEs vary across slices throughout the scanned region.[13] CT manufacturers have begun displaying estimated SSDE values alongside other dosimetry quantities, but these features often incur additional costs. Furthermore, different CT manufacturers incorporate proprietary algorithms within their software to estimate D_w and SSDEs. Variations in computational methods across manufacturers may lead to discrepancies in reported D_w values, potentially affecting SSDE calculations and radiation dose assessments. In some manufacturers' software, the SSDE (geometrical) is displayed as an estimate of the radiation dose a patient receives from a CT scan. This estimate is calculated using the patient's dimensions, such as the effective diameter to derive a conversion factor from $CTDI_{vol}$, rather than using the D_w as the primary metric. Moreover, the SSDE value displayed by CT scanners is often a single value, representing either an average across the scanned region or a measurement from the middle slice. This approach limits the ability of users to assess the SSDE for individual slices, which may more accurately reflect localized radiation absorption. As a result, non-commercial automated solutions have gained popularity. Some studies have developed automated programs to calculate SSDEs; however, many of these lack direct comparison with established methods, making it difficult to confirm their validity and clinical reliability.[14-16] In this study, we developed and validated a user-friendly computational tool for estimating slice-specific D_w, $CTDI_{vol}$, and SSDEs, based on methodologies outlined in AAPM reports. A custom ImageJ macro was created to perform automated, threshold-based body contour segmentation and extract slice-specific exposure values directly from Digital Imaging and Communications in Medicine (DICOM) metadata. The accuracy and clinical relevance of the method were evaluated through comparison with both commercial CT scanner outputs and dose monitoring software using phantom and patient datasets. This approach provides an accessible and transparent solution for patient-specific dose estimation, enabling detailed slice-by-slice assessment and offering greater spatial resolution than conventional scanner displays or commercial software systems.

Main points

- A custom ImageJ macro was developed to automatically calculate the slice-specific volume computed tomography (CT) dose index ($CTDI_{vol}$), water-equivalent diameter, and size-specific dose estimate (SSDE) from CT images.
- The macro exhibited excellent agreement with both scanner console values and commercial software (Radimetrics), especially for $CTDI_{vol}$ and SSDE.
- Slice-by-slice dose evaluation revealed dose variations that are not visible in conventional average-based reporting.
- This method allows detailed, patient-specific dose assessment and supports protocol optimization in clinical and research settings.
- The tool is low cost, open source, and suitable for institutions without access to commercial dose monitoring systems.

Methods

CT imaging was performed using both homogeneous circular phantoms and anthropomorphic phantoms representing the head, thorax, and abdomen. All phantom scans were conducted using the Siemens SOMATOM go.Top® scanner (Siemens Healthineers, Erlangen, Germany).

In addition, clinical CT datasets were retrospectively collected from at least 30 patients who underwent routine head, chest, and abdomen examinations in accordance with the hospital's standard imaging protocols. Two CT scanners were involved in data collection. For Scanner A (Siemens SOMATOM go.Top®), the $CTDI_{vol}$, D_w, and SSDE values were recorded directly from the scanner console. For Scanner B (Siemens SOMATOM Force®), the corresponding dose parameters were extracted using Radimetrics, a commercial dose monitoring software integrated with the scanner.

Development of ImageJ macro for slice-specific dose calculations

A custom macro was developed using ImageJ (version 1.54g, National Institutes of Health, Bethesda, MD, USA)[17] to estimate the SSDE from DICOM-format CT image stacks, in accordance with the guidelines provided by AAPM reports 220 and 293.

Data acquisition and preprocessing

CT image datasets were acquired from a Siemens SOMATOM scanner (syngo CT VA40A software) and SOMATOM force, and DICOM files were imported into ImageJ as image stacks, each representing a series of con-

tiguous axial slices from either head or body examinations. Prior to analysis, metadata, including the number of slices, slice location, and exposure (DICOM tag 0018,1152—"Exposure"), were extracted using the ImageJ DICOM header parser.

Body contour segmentation and area calculation

To estimate patient size (D_w), each slice underwent automatic body contour segmentation using a threshold-based method. A threshold of –140 Hounsfield unit (HU) was applied to segment the patient's body contour, effectively distinguishing body tissues from the surrounding air to enable consistent and reproducible D_w measurements. This threshold has been successfully applied in previous SSDE-related studies in CT examinations[18] and was selected to balance the exclusion of air while avoiding inclusion of the scanner couch. Although lower thresholds (–300 to –500 HU) have been employed in other pipelines, such as the CT contour (–383 HU) for abdomen–pelvic CT,[19] these have been reported to occasionally include couch structures, potentially reducing contour accuracy. After segmentation, the "Analyze Particles" function in ImageJ was used to detect regions of interest (ROIs), with size and circularity constraints (size: 5000–∞ pixels, circularity: 0.2–1.0) to exclude non-patient structures such as the scanner couch. The cross-sectional area (A) of each ROI was then calculated based on pixel spacing from the DICOM metadata.

Slice-specific water-equivalent diameter calculation

For each slice, the D_w was calculated from the segmented area and average CT number within the ROI, as follows:

$$D_w = 2\sqrt{\left[\frac{1}{1000}\overline{CT(x,y)_{ROI}} + 1\right]\frac{A_{ROI}}{\pi}} \quad \text{Eq.1}$$

where D_w is the water-equivalent diameter (cm), $\overline{CT(x,y)_{ROI}}$ is the average CT number within the area of interest, and is the area of the ROI (cm^2).

Size-specific dose estimate calculation

The slice-specific SSDE was calculated as follows:

$$SSDE = CTDI_{vol} \times f \quad \text{Eq.2}$$

The correction factor (*f*) was determined from the calculated D_w value, accounting for variations in patient size and scanner phantom type. Separate exponential functions were applied depending on whether $CTDI_{vol}$ was derived from a 16- or 32-cm calibration phantom, with the source equations taken from AAPM Report 293 for head examinations[9] and AAPM Report 220 for body examinations[8]:

$$f^{H16} = 1.9852e^{(-0.0486D_w)} \quad \text{Eq.3}$$
$$f^{B32} = 3.7055e^{(-0.0367D_w)} \quad \text{Eq.4}$$

where *H16* and *B32* nomenclature are used in the superscript of the conversion factor *f* when 16- or 32-cm CTDI phantoms were used for the head (*H*) or body (*B*) $CTDI_{vol}$ measurements and D_w is the water-equivalent diameter.

$$CTDI_{vol,slice} = \left(\frac{Exposure_{slice}}{Exposure_{avg}}\right) \times CTDI_{vol,avg} \quad \text{Eq.5}$$

The slice-specific $CTDI_{vol}$ ($CTDI_{vol,slice}$) was estimated by normalizing the scanner-displayed $CTDI_{vol}$ to the exposure value of each slice) ($CTDI_{vol,avg}$) The exposure value (tag 0018,1152) represents the tube current–time product in mAs, where $Exposure_{slice}$ refers to the tube current–time product for that particular slice and $Exposure_{avg}$ refers to the average tube current–time product across the entire scan.

Finally, SSDE per slice ($SSDE_{slice}$) was calculated as follows:

$$SSDE_{slice} = CTDI_{vol,slice} \times f_{corr} \quad \text{Eq.6}$$

where f_{corr} is the correction factor corresponding to the slice-specific D_w and scan region (head or body).

The macro generated an output table containing the following parameters for each slice: slice location, exposure, segmented area, mean pixel value, D_w, correction factor, $CTDI_{vol}$ per slice, and SSDE per slice. All calculations were performed in real time within the ImageJ environment and exported to CSV format for further statistical analysis.

Data comparison and statistical analysis

Statistical analyses were performed using Stata version 17 (StataCorp, College Station, TX, USA). Agreement between $CTDI_{vol}$, D_w, and SSDE values obtained from the custom ImageJ macro and those from the scanner console and Radimetrics software was assessed using intraclass correlation coefficients (ICCs) and Bland–Altman plots. Specifically, ICC (3,1), a two-way mixed-effects model for absolute agreement with single measurements, was employed. Interpretation of ICC values followed established guidelines: <0.5 = poor agreement, 0.5–0.75 = moderate agreement, 0.75–0.9 = good agreement, and >0.9 = excellent agreement.

Research ethics standards compliance

This retrospective study was approved by the Institutional Review Board (IRB) under expedited review (COA No. 081/2025) on March 18, 2025. All CT images were originally acquired for clinical purposes and were fully anonymized before being retrospectively analyzed, with no identifiable patient information included. As the CT images were already taken for routine medical care and later de-identified, the IRB waived the requirement for obtaining informed consent in accordance with ethical guidelines for retrospective studies.

Results

Development of the dose calculation macro

The study population is presented in Figure 1a. The workflow of the macro is illustrated in Figure 1b, showing sequential steps from image input, DICOM metadata extraction, ROI detection, dose calculations, and final data export.

An ImageJ macro was successfully developed to calculate slice-specific dose metrics from CT images. The tool automatically segments the patient contour on each slice using a –140 HU threshold, calculates D_w, and determines slice-specific $CTDI_{vol}$ and $CTDI_{vol,slice}$ based on DICOM exposure values (tag 0018,1152). The SSDE is then computed for each slice using the appropriate correction factors from AAPM reports. The macro completes analysis in approximately 30 seconds per examination, providing comprehensive output including the slice location, exposure, area, D_w, correction factor, $CTDI_{vol}$, and SSDE for each slice.

Validation of the macro with phantom studies

The accuracy of the macro-calculated D_w and SSDE values was validated against scanner-displayed measurements using both uniform water phantoms and anthropomorphic phantoms. The results for water phantoms of different sizes (16 and 19 cm inner diameter) are presented in Table 1, showing excellent agreement with differences of less than 2.3% for both D_w and SSDE measurements.

For anthropomorphic phantoms of the head, chest, and abdomen (Table 2), the macro demonstrated comparable accuracy. In the head phantom, both the middle-slice and average values closely matched the scanner output. The chest phantom showed

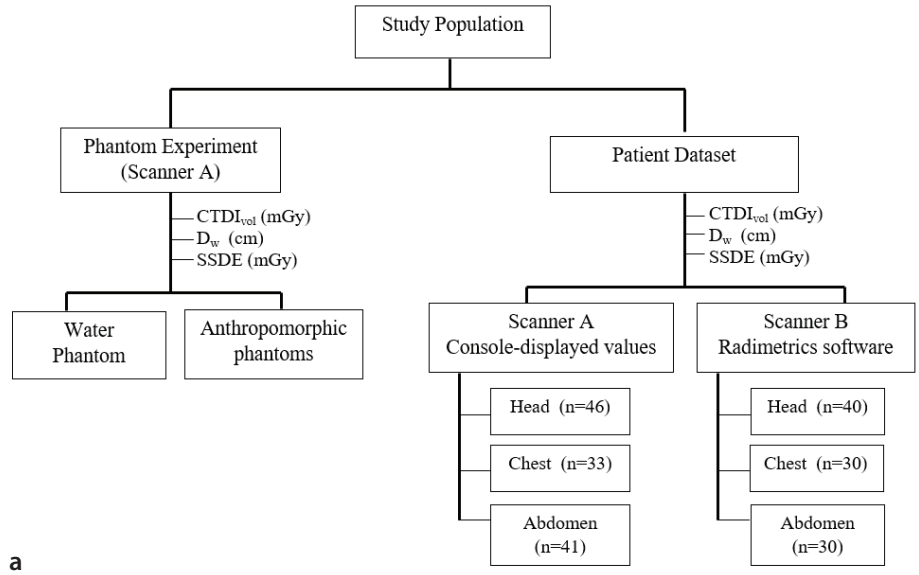

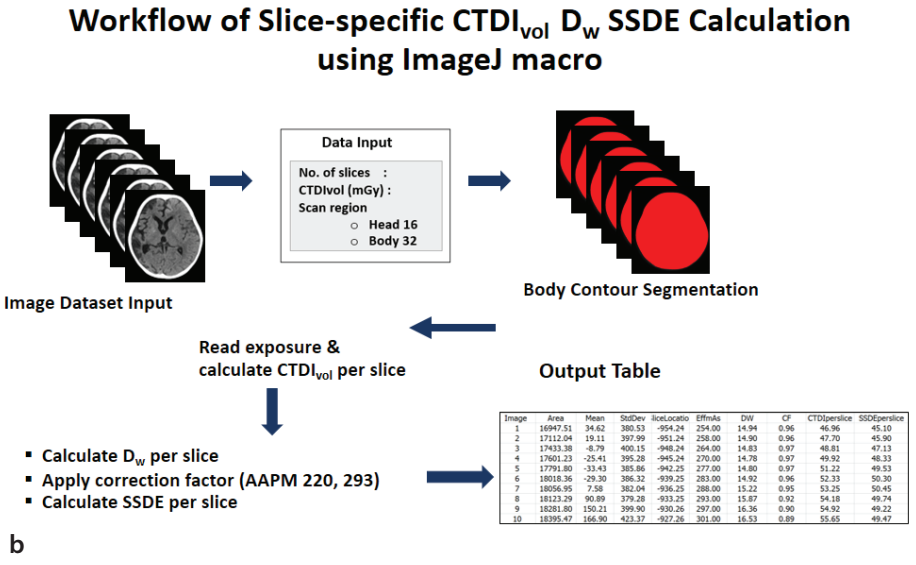

Figure 1. **(a)** The study population, and **(b)** the workflow for automated slice-specific calculation of the volume computed tomography dose index, water-equivalent diameter, and size-specific dose estimate using the ImageJ macro. $CTDI_{vol}$, volume computed tomography dose index; D_w, water-equivalent diameter; SSDE, size-specific dose estimate.

the most pronounced slice-to-slice variation in SSDE (range: 5.77–23.68 mGy) despite the average value (12.56 ± 6.99 mGy) being nearly identical to the scanner-reported value (12.5 mGy). This key variation highlights the importance of slice-specific dose assessment in anatomically heterogeneous regions. The abdomen phantom showed more consistent values across slices, with average measurements within 5% of scanner-displayed values.

These validation studies confirm that the macro provides accurate D_w and SSDE calculations that align well with scanner-reported values while offering the additional advantage of slice-specific analysis that reveals dose distribution patterns not captured by console-displayed averages.

Analysis of clinical patient scans

Scanner A

Agreement between the automated slice-specific dose calculations and the scanner-displayed values from Scanner A (Siemens SOMATOM go.Top®) was evaluated using Bland–Altman analysis and ICCs. The comparison included three dose parameters—$CTDI_{vol}$, D_w, and SSDE—assessed separately for head and chest/abdomen scans.

The Bland–Altman analysis shown in Table 3 and plots shown in Figure 2 demonstrate excellent overall agreement between the ImageJ macro and the scanner-reported values. For head scans, the mean differences between the macro-derived and scanner-reported values were 2.285 mGy for $CTDI_{vol}$, 0.649 cm for D_w, and −1.670 mGy for the SSDE, with 95% limits of agreement indicating acceptable variability. Similarly, for chest and abdomen scans, the mean differences were −0.001 mGy, −0.336 cm, and 0.284 mGy, respectively, within clinically acceptable ranges.

These findings were further supported by ICC analysis. The ICC (3,1) values for $CTDI_{vol}$, D_w, and the SSDE for head scans were 0.974, 0.893, and 0.965, respectively, indicating good to excellent agreement. For chest and abdomen scans, ICC (3,1) values were 1.000 for $CTDI_{vol}$, 0.994 for D_w, and 0.989 for the SSDE, also reflecting excellent agreement across methods.

Scanner B

The Bland–Altman analysis (Table 3 and Figure 3) for head CT showed a mean difference in $CTDI_{vol}$ of 0.067 mGy, with 95% limits of agreement from −0.653 to 0.787 mGy and an ICC (3,1) of 0.996. For the SSDE, the mean difference was −0.123 mGy (−1.911 to 1.665 mGy), with an ICC of 0.967, confirming near-perfect agreement between the ImageJ macro and Radimetrics for head scans on Scanner B. By contrast, D_w demonstrated poor agreement, with a mean difference of 1.250 cm (0.609 to 1.890 cm) and an ICC of 0.267. This discrepancy highlights a potential risk of misestimating patient size and dose if console-reported D_w is used alone; however, the SSDE values maintained near-perfect agreement (ICC: 0.967), underscoring its robustness as a clinically relevant dose metric.

For chest/abdomen CT, the mean difference in $CTDI_{vol}$ was −0.014 mGy, with limits of agreement ranging from −0.1 to 0.072 mGy and an ICC of 1.000. The D_w comparison showed a mean difference of −0.312 cm (−2.577 to 1.954 cm), with an ICC of 0.94. The SSDE values differed by a mean of −0.119 mGy (−4.670 to 4.432 mGy), and the ICC was 0.884.

A comparative analysis of D_w and SSDE values between the CT console output and the ImageJ macro for the two scanners across the head, chest, and abdomen regions is shown in Figure 4. For Scanner A, the macro slightly overestimated D_w in the head region [mean ± standard deviation (SD): 15.8 ± 1.4 vs. 15.2 ± 1.5 cm]; this was similar for Scanner B, with higher macro values (17.2 ± 0.6 vs. 16.0 ± 0.6 cm). In the chest and abdomen, the differences were minor, with both scanners showing close agreement between methods.

Table 1. Comparison of D_w and SSDE values between CT scanner output and automated calculation in water phantoms

Phantom	$CTDI_{vol}$ (mGy)	CT scanner		Automated calculations	
		D_w (cm)	SSDE (mGy)	D_w (cm)	SSDE (mGy)
Small water phantom*	37.5	16.5	33.4	16.75	33.00
Large water phantom**	37.5	19.5	28.9	19.95	28.24

Scan protocol, 120 kV; effective mAs, 410; field of view, 300 mm; pitch, 1.0; slice thickness, 3 mm; convolution kernel, Hr40; * D_{Eff} =16 cm and D_{Eff} includes outer shell = 17 cm; ** D_{Eff} =19 cm and D_{Eff} includes outer shell = 20 cm. CT, computed tomography; $CTDI_{vol}$, volume computed tomography dose index; D_w, water-equivalent diameter; SSDE, size-specific dose estimate.

Table 2. Comparison of D_w and SSDE from CT scanner display and automated calculations using the developed macro in head, chest, and abdomen phantoms

Phantom	D_w (cm)			$CTDI_{vol}$ (mGy)			SSDE (mGy)		
	CT scanner display	Automated calculations (MS)	Automated calculations (ASA)	CT scanner display	Automated calculations (MS)	Automated calculations (ASA)	CT scanner display	Automated calculations (MS)	Automated calculations (ASA)
Head	16.2	18.47	16.46 ± 2.75 (6.76 – 18.91)	50.6	60.16	55.41 ± 5.54 (37.48 – 60.53)	49.2	48.73	49.19 ± 1.44 (46.34 – 53.60)
Chest	22.3	22.38	22.29 ± 2.60 (13.65 – 25.22)	7.4	4.73	7.85 ± 4.69 (2.76 – 15.33)	12.5	7.70	12.56 ± 6.99 (5.77 – 23.68)
Abdomen	26.4	28.01	27.20 ± 1.55 (24.94 – 29.54)	7.09	7.22	7.15 ± 1.14 (5.53 – 8.74)	10.1	9.60	9.70 ± 1.13 (8.07 – 11.66)

Head protocol, 120 kV; effective mAs, 410; field of view (FOV), 250 mm; pitch, 0.55; slice thickness, 3 mm; convolution kernel, Hr40; SAFIRE strength level 3.
Chest protocol, 120 kV; effective mAs, 125; FOV, 400 mm; pitch, 0.8; slice thickness, 3 mm; convolution kernel, Hr40; SAFIRE strength level 3.
Abdomen protocol, 120 kV; effective mAs, 180; FOV, 400 mm; pitch, 0.8; slice thickness, 3 mm; convolution kernel, Hr40; SAFIRE strength level 3.
CT, computed tomography; $CTDI_{vol}$: volume computed tomography dose index, D_w, water-equivalent diameter; SSDE: size-specific dose estimate; MS, middle slice of scan length; ASA, all slices average.

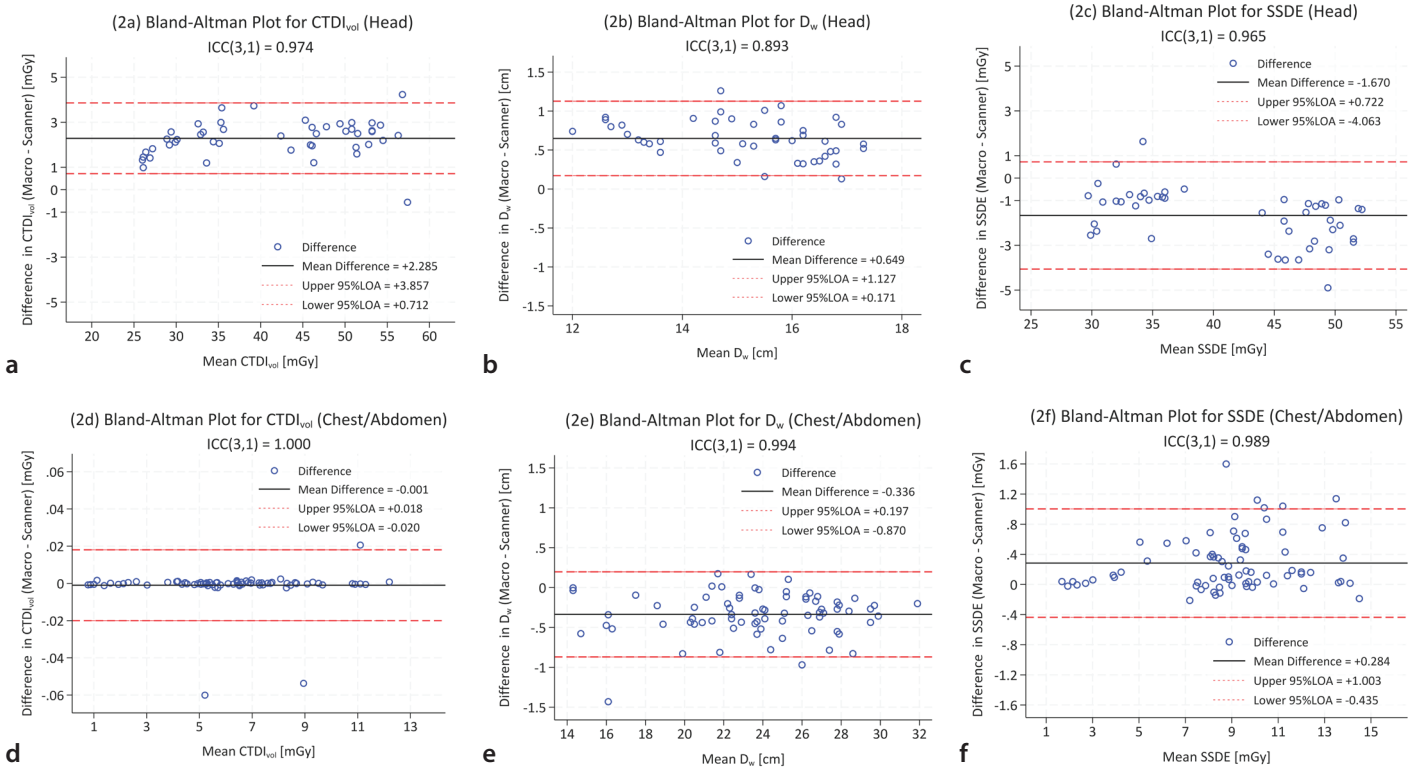

Figure 2. Bland–Altman plots comparing the dose parameters obtained from the ImageJ macro and the scanner console display (Scanner A) for **(a)** volume computed tomography dose index ($CTDI_{vol}$), **(b)** water-equivalent diameter (D_w), and **(c)** size-specific dose estimate (SSDE) in head computed tomography (CT) examinations and **(d)** $CTDI_{vol}$, **(e)** D_w, and **(f)** SSDE in chest/abdomen CT examinations. LOA, limits of agreement; ICC, intraclass correlation coefficient.

Table 3. Bland–Altman analysis and intraclass correlation coefficients (ICCs) comparing $CTDI_{vol}$, D_w, and SSDEs between the ImageJ macro and scanner console (Scanner A) and Radimetrics (Scanner B)

Scanner	CT exam		Bland & Altman			ICC (3,1)			
			Mean difference	Lower 95% LOA	Upper 95% LOA	Individual ICC	Lower 95% CI	Upper 95% CI	*P* value
A	Head (n = 46)	$CTDI_{vol}$ (mGy)	+2.285	+0.712	+3.857	0.974	0.084	0.995	<0.001
		D_w (cm)	+0.649	+0.171	+1.127	0.893	−0.022	0.976	<0.001
		SSDE (mGy)	−1.670	−4.063	+0.722	0.965	0.481	0.991	<0.001
	Chest/abdomen (n = 74)	$CTDI_{vol}$ (mGy)	−0.001	−0.020	+0.018	1.000	1.000	1.000	<0.001
		D_w (cm)	−0.336	−0.870	+0.197	0.994	0.906	0.998	<0.001
		SSDE (mGy)	+0.284	−0.435	+1.003	0.989	0.952	0.995	<0.001
B	Head (n = 40)	$CTDI_{vol}$ (mGy)	+0.067	−0.653	+0.787	0.996	0.992	0.998	<0.001
		D_w (cm)	+1.250	+0.609	+1.890	0.267	−0.030	0.658	<0.001
		SSDE (mGy)	−0.123	−1.911	+1.665	0.967	0.933	0.984	<0.001
	Chest/abdomen (n = 60)	$CTDI_{vol}$ (mGy)	−0.014	−0.100	+0.072	1.000	1.000	1.000	<0.001
		D_w (cm)	−0.312	−2.577	+1.954	0.940	0.899	0.964	<0.001
		SSDE (mGy)	−0.119	−4.670	+4.432	0.884	0.812	0.929	<0.001

CT, computed tomography; $CTDI_{vol}$, volume computed tomography dose index; D_w, water-equivalent diameter; SSDE, size-specific dose estimate; LOA, limits of agreement; CI, Confidence interval.

Macro-derived SSDE values closely matched those from the console. In head CT scans, Scanner A showed a mean SSDE value of 39.8 ± 7.5 (macro) and 41.4 ± 8.0 mGy (console), whereas Scanner B yielded 38.3 ± 3.6 (macro) and 38.5 ± 3.5 mGy (console). For the chest and abdomen, differences were minor for Scanner A; however, for Scanner B, slightly greater differences were observed: mean chest SSDEs of 13.5 ± 4.0 (macro) and 12.0 ± 3.3 mGy (console), and mean abdomen SSDEs of 16.7 ± 4.3 (macro) and 18.3 ± 4.6 mGy (console).

Larger variations were observed in the chest and abdomen for Scanner B than for Scanner A, with Bland–Altman analysis showing 95% limits of agreement from –4.670 to +4.432 mGy (Figure 3f) compared with –0.435 to +1.003 mGy for Scanner A (Figure 2f). Nevertheless, mean SSDE differences between the macro and console for Scanner B were minimal, with relative deviations of 0.52% for head CT and 0.66% for chest/abdomen CT, both well below the ± 10% threshold generally considered acceptable for clinical dose estimation.

Discussion

It is important to emphasize that $CTDI_{vol}$, DLP, and the SSDE are not intended to represent actual absorbed doses in individual patients; rather, these dose indicators are designed for quality assurance (QA), dose tracking, and protocol optimization, as recommended by the AAPM.

However, conventional metrics such as $CTDI_{vol}$ and DLP reflect only averaged values across the entire scan range, potentially masking substantial intra-scan dose variations. To address this limitation, we developed and validated an ImageJ macro capable of slice-specific dose estimation. By generating spatially resolved $CTDI_{vol}$, D_w, and SSDE values, the macro enhances the granularity of dose reporting and enables identification of within-scan dose fluctuations that may be clinically relevant.

Although DLP provides a cumulative measure of radiation output over the scanned region, it lacks spatial resolution. By contrast, the slice-specific $CTDI_{vol}$ values derived using our tool offer a detailed map of dose distribution along the z-axis. This capability allows for the identification of peak dose regions—commonly occurring at anatomical transitions such as the shoulders or skull base—and provides valuable data for tailoring protocols or conducting organ-level dosimetric studies.

Comparison between the developed macro and siemens console display

The ImageJ macro developed in this study provides patient-specific, slice-by-slice analysis of CT dose parameters, offering higher granularity than the Siemens console display. Although the console reports effective mAs, $CTDI_{vol}$, and SSDEs as modulation-weighted averages or values from a representative slice, these measurements do not capture anatomical variations throughout the scan range. By contrast, the macro calculates $CTDI_{vol}$ and SSDE per slice using exposure data extracted from DICOM metadata (tag 0018,1152) and cross-sectional area measurements (D_w) obtained through threshold-based segmentation.

This difference was particularly evident in head CT examinations, where substantial anatomical variation exists between the vertex and skull base. The slice-by-slice approach provided more detailed SSDEs, revealing dose variations that are not apparent in the averaged values shown on the scanner console. Notably, discrepancies of 15%–35% were observed at anatomical transition zones, such as the thoracoabdominal junction, where rapid changes in cross-sectional area occur.

Another key difference involves the handling of tube current modulation. The Siemens console provides only averaged effective mAs for the entire scan, whereas the macro captures actual slice-specific exposure values, reflecting real-time adjustments in tube current. This capability allows for more precise dose estimation, particularly for modern protocols that employ aggressive modulation techniques.

The macro also offers temporal resolution advantages by generating comprehensive dose profiles across the scan range, enabling identification of dose peaks and facilitating protocol optimization. Although console-displayed metrics remain useful for rapid dose feedback and protocol adjustments in clinical workflows, they typically provide only a single averaged value. By contrast, the macro yields high-resolution, slice-specific dose estimates that reveal otherwise obscured intra-scan dose variations not cap-

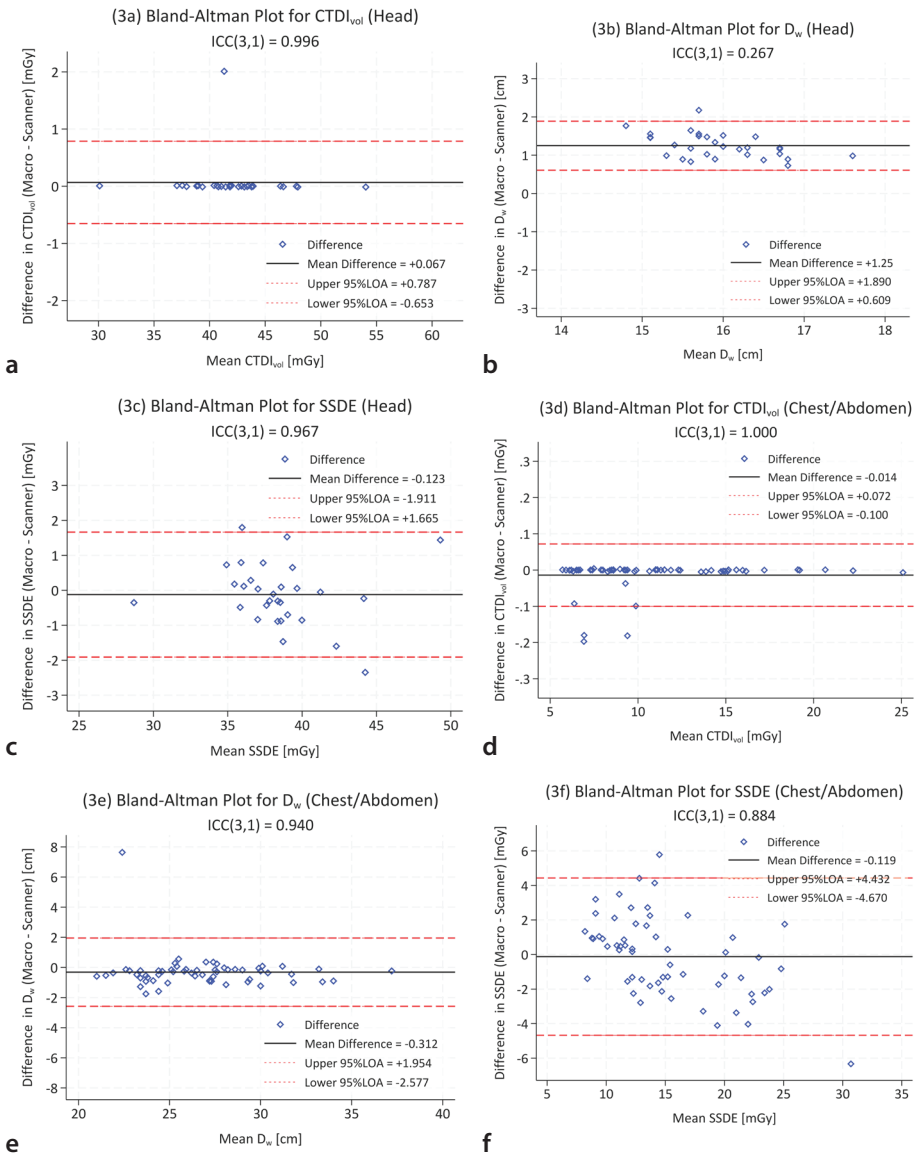

Figure 3. Bland–Altman plots comparing the dose parameters obtained from the ImageJ macro and Radimetrics (Scanner B) for **(a)** volume computed tomography dose index ($CTDI_{vol}$), **(b)** water-equivalent diameter (D_w), and **(c)** size-specific dose estimate (SSDE) in head computed tomography (CT) examinations and **(d)** $CTDI_{vol}$, **(e)** D_w, and **(f)** SSDE in chest/abdomen CT examinations. LOA, limits of agreement; ICC, intraclass correlation coefficient.

tured by conventional summary metrics, a feature particularly valuable in anatomically heterogeneous regions such as the thorax and pelvis.

Comparison between the developed imagej macro and commercial dose monitoring software (Radimetrics)

Considerable methodological and functional differences were observed between the developed ImageJ macro and the commercial dose monitoring software Radimetrics™ (Bayer Healthcare). Although both systems extract dose-relevant information from DICOM headers and estimate patient-specific dose metrics, the processes, assumptions, and applications differ substantially.

The observed differences in D_w agreement between anatomical regions can be attributed to distinct threshold segmentation approaches. Our ImageJ macro uses a fixed threshold of −140 HU; by contrast, although the exact threshold values used by commercial dose management systems such as Radimetrics are not publicly disclosed, several studies and indirect validations suggest that these systems commonly apply a body contour segmentation threshold in the range of approximately −300 to −500 HU. This threshold range is designed to avoid including excessive air (below −500 HU) while preventing the exclusion of soft tissue (above −300 HU).

The anatomical differences substantially influence the impact of threshold selection on D_w calculation. In head CT, the relatively uniform soft tissue density and distinct bone–air interfaces make D_w particularly sensitive to segmentation. For example, a threshold of −140 HU (as used in our macro) may inadvertently exclude bone edges or include small air pockets, leading to substantial changes in mean CT numbers within the ROI and consequently affecting D_w calculations, in accordance with AAPM 220 methodology. Similarly, lower thresholds within the range applied by commercial systems (−300 to −500 HU, e.g., −400 HU) have also been reported to occasionally include couch structures. These threshold-related factors explain the poor agreement (ICC = 0.267) observed for head D_w measurements.

Conversely, in chest and abdomen CT, the more heterogeneous tissue composition and larger soft tissue volumes make the calculations less sensitive to threshold variations. The predominance of soft tissue in these regions provides more stable mean CT numbers, resulting in improved D_w agreement (ICC = 0.940) despite different threshold approaches.

Quantitative comparison between the two systems using Bland–Altman plots and ICC analysis reflects these methodological differences. For head CT examinations, although $CTDI_{vol}$ and SSDEs showed near-perfect agreement with ICC values of 0.996 and 0.967, respectively, D_w demonstrated poor agreement (IC: 0.267), with a mean difference of 1.25 cm. This substantial discrepancy likely stems from the different threshold segmentation approaches affecting the CT number-based calculations more substantially in the relatively homogeneous head anatomy. Nevertheless, SSDEs remained robust despite this variability in D_w, as the exponential correction factor $f(D_w)$ changes only gradually in the head diameter range, limiting the propagation of D_w errors into SSDEs. Together with the near-perfect agreement in $CTDI_{vol}$, this explains the consistently high SSDE agreement observed for head CT examinations.

For chest/abdomen scans, the agreement was more consistent across all parameters: $CTDI_{vol}$ showed excellent agreement, with an ICC of 1.00 and mean difference of −0.014 mGy; D_w comparison yielded good agreement (ICC: 0.940), with a mean difference of −0.312 cm; and SSDEs showed excellent agreement (ICC: 0.884), with a mean difference of −0.119 mGy. This suggests that the heterogeneous tissue composition in these regions provides more robust results despite methodological differences.

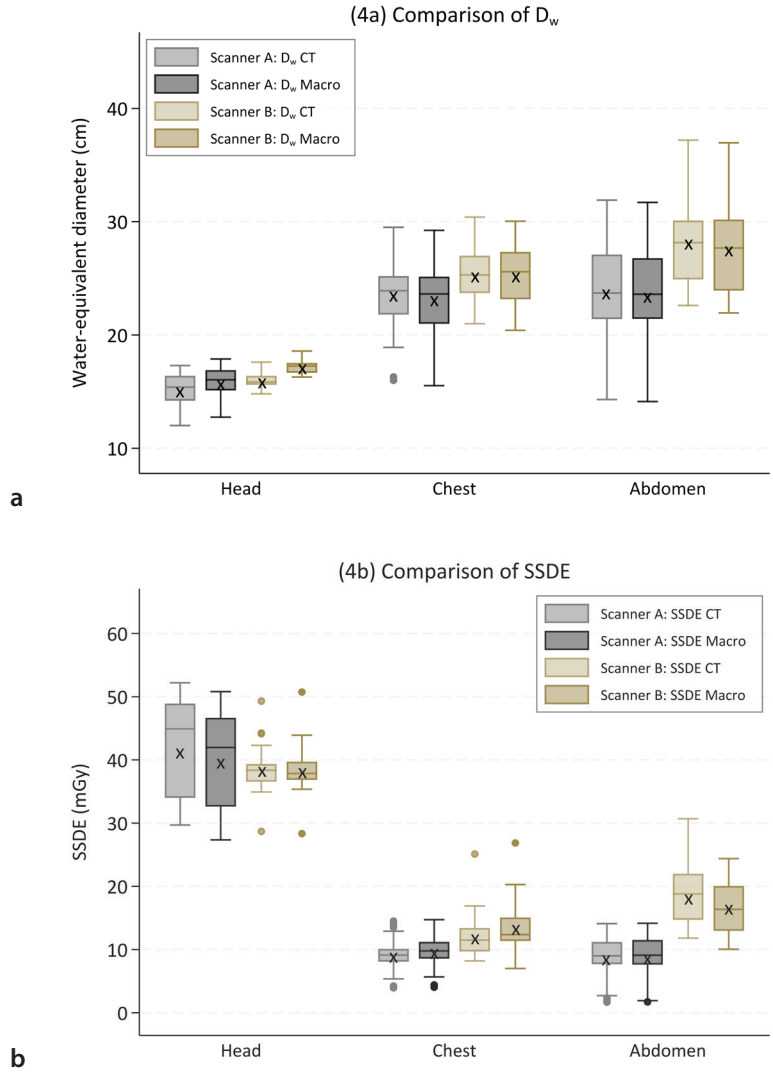

Figure 4. Box plot comparison of **(a)** the water-equivalent diameter and **(b)** size-specific dose estimate obtained from the ImageJ macro, computed tomography scanner console, and Radimetrics across anatomical regions and scanners. Boxes represent the interquartile range, center lines indicate the median, whiskers extend to the data range, and crosses (×) represent the mean values. CT, computed tomography; D_w, water-equivalent diameter; SSDE, size-specific dose estimate.

The macro's threshold-based segmentation was validated using phantoms and yielded results within 5% of physical dimensions while requiring fewer computational resources. However, challenges such as low-contrast boundaries (e.g., at air–bone interfaces) can reduce accuracy in specific regions such as the head. These findings highlight the importance of understanding the underlying algorithmic differences when comparing dose monitoring systems. The threshold-dependent nature of D_w calculations, particularly in anatomically uniform regions such as the head, suggests that standardization of segmentation approaches may be necessary for consistent inter-system comparisons.

From a practical standpoint, Radimetrics excels in enterprise-wide integration. It automatically processes all CT examinations without user interaction and provides compliance dashboards and centralized QA tools. By contrast, the ImageJ macro requires manual execution, input selection, and parameter adjustment. Although this limits automation, it offers unmatched flexibility for protocol-specific analysis, research customization, and pediatric dose assessment. In terms of cost, the macro presents a clear advantage. Commercial systems such as Radimetrics require considerable investment in licensing, infrastructure, and ongoing support. The macro, built entirely on open-source tools, is a cost-effective alternative for institutions with research goals, limited budgets, or custom analysis needs.

Practical considerations for clinical implementation

Significant differences in D_w and SSDEs were observed in chest and abdomen scans, likely due to variations in field-of-view (FOV) settings. In some cases, the FOV may not fully cover the patient's body cross section, particularly at the lateral margins, leading to underestimation of body size in image-based calculations. This effect may be more pronounced in larger or misaligned patients.

Despite being statistically significant, these differences are generally within ± 10% and may have limited clinical impact, as key organs typically remain within the scan range. To reduce such discrepancies, consistent patient positioning and standardized FOV protocols are essential. Regular QA processes should validate dose calculation accuracy across various scanning conditions. Further studies in broader patient groups, including pediatric and atypical body types, are recommended to ensure the robustness of SSDEs.

Clinical implication of slice-specific dose estimates for protocol optimization

The granularity provided by slice-specific SSDEs offers critical insight into dose heterogeneity along the scan length. For instance, anatomical regions such as the shoulders or skull base often exhibit elevated SSDE values due to increased patient attenuation, which can trigger ATCM to deliver higher output. Conversely, areas such as the lungs or extremities may receive lower doses. Identifying these "higher" or "lower" dose sections allows radiology teams to fine-tune scan protocols accordingly.

For high-dose regions, protocol adjustments may involve reducing the maximum tube current limit, modifying ATCM curves, adjusting the noise index, or narrowing z-axis coverage if clinically acceptable. By contrast, persistently low-dose areas—especially those critical to diagnosis—may benefit from increased minimum mA thresholds, longer rotation times, or customized reconstruction parameters to preserve image quality. Such region-specific refinement, when guided by slice-level SSDE data and supported by institutional or national diagnostic reference levels, enables a more personalized approach to CT protocol design. Ultimately, this facilitates a balance between diagnostic performance and radiation safety.

This study has several limitations. The use of a fixed threshold (–140 HU) may not be optimal for all anatomical regions, particularly in low-contrast boundaries such as air–bone interfaces in head CT, where D_w accuracy may be affected. Future work could explore adaptive or data-driven thresholding approaches to improve segmentation performance across diverse anatomies, thereby enhancing the robustness and clinical applicability of the tool. Validation was limited to Siemens scanners and Radimetrics software; testing with other vendors (e.g., GE, Philips, Canon) is needed to assess broader applicability. The clinical dataset included only 30 patients, restricting variability in body size, pathology, and scan protocols. Inter-observer variability in manual parameter settings was not evaluated, which may affect reproducibility. Additionally, the macro currently lacks automated quality checks and standardized reporting, limiting its readiness for routine clinical integration. Moreover, we did not compare scanner-reported DLP values with the cumulative $CTDI_{vol}$ from the macro, as the precise irradiation length used by the scanner was not available in the DICOM metadata. Since DLP calculation depends on irradiation length, which may differ from the reconstructed scan length due to overscanning or collimation, direct comparisons would be inaccurate or misleading. Therefore, instead of focusing on DLP comparison, our study emphasizes the added value of slice-specific $CTDI_{vol}$ analysis, which reveals spatial variations in dose that global metrics such as DLP or average $CTDI_{vol}$ cannot capture. Future development should address automation, segmentation robustness, cross-vendor compatibility, and streamlined clinical implementation.

In conclusion, the developed ImageJ macro enables automated, slice-specific calculation of $CTDI_{vol}$, D_w, and SSDEs with high agreement with scanner and commercial software outputs. Its ability to reveal intra-scan dose variations offers improved slice-by-slice information for dose assessment and supports protocol optimization in clinical and research settings.

Acknowledgments

The authors would like to express their sincere gratitude to Kamphaeng Phet Hospital and Bumrungrad International Hospital for their valuable contribution in providing clinical data essential for this research. Their cooperation and support were instrumental in the successful completion of this study. The authors also gratefully acknowledge Buddhachinaraj Hospital, Phitsanulok, for providing access to Stata version 17 software used in the statistical analysis.

Footnotes

Conflict of interest disclosure

The authors declared no conflicts of interest.

References

1. Bos D, Guberina N, Zensen S, Opitz M, Forsting M, Wetter A. Radiation exposure in computed tomography. *Dtsch Arztebl Int*. 2023;120(9):135-141. [Crossref]
2. Burtt JJ, Thompson PA, Lafrenie RM. Non-targeted effects and radiation-induced carcinogenesis: a review. *J Radiol Prot*. 2016;36(1):R23-35. [Crossref]
3. Hedgire S, Ghoshhajra B, Kalra M. Dose optimization in cardiac CT. *Phys Med*. 2017;41:97-103. [Crossref]
4. Huda W, Mettler FA. Volume CT dose index and dose-length product displayed during CT: what good are they? *Radiology*. 2011;258(1):236-242. [Crossref]
5. Durand DJ, Mahesh M. Understanding CT dose display. *J Am Coll Radiol*. 2012;9(9):669-671. [Crossref]
6. McCollough CH, Leng S, Yu L, Cody DD, Boone JM, McNitt-Gray MF. CT dose index and patient dose: they are not the same thing. *Radiology*. 2011;259(2):311-316. [Crossref]
7. American Association of Physicists in Medicine (AAPM). Size-specific dose estimates (SSDE) in pediatric and adult body CT examinations. In: AAPM Report No. 204. College Park, MD: American Association of Physicists in Medicine; 2011. [Crossref]
8. American Association of Physicists in Medicine (AAPM). Use of water equivalent diameter for calculating patient size and size-specific dose estimates (SSDE) in CT. In: AAPM Report No. 220. College Park, MD: American Association of Physicists in Medicine; 2014. [Crossref]
9. American Association of Physicists in Medicine (AAPM). AAPM task group 293: Size-specific dose estimates (SSDE) for body CT examinations based on effective diameter and water-equivalent diameter. In: AAPM Report No. 293. College Park, MD: American Association of Physicists in Medicine; 2023. [Crossref]
10. Abdulkadir MK, Osman ND, Achuthan A, et al. A segmentation-based automated calculation of patient size and size-specific dose estimates in pediatric computed tomography scans. *J Med Phys*. 2024;49(3):456-463. [Crossref]
11. Moore BM, Brady SL, Mirro AE, Kaufman RA. Size-specific dose estimate (SSDE) provides a simple method to calculate organ dose for pediatric CT examinations. *Med Phys*. 2014;41(7):071917. [Crossref]
12. McMillan K, Bostani M, Cagnon C, Zankl M, Sepahdari AR, McNitt-Gray M. Size-specific, scanner-independent organ dose estimates in contiguous axial and helical head CT examinations. *Med Phys*. 2014;41(12):121909. [Crossref]
13. Sookpeng S, Martin CJ, Krisanachinda A. Design and use of a phantom for testing and comparing the performance of computed tomography automatic tube current modulation systems. *J Radiol Prot*. 2020;40(3):753-773. [Crossref]
14. Anam C, Haryanto F, Widita R, Arif I, Dougherty G. Automated calculation of water-equivalent diameter (DW) based on AAPM task group 220. *J Appl Clin Med Phys*. 2016;17(4):320-333. [Crossref]
15. Anam C, Mahdani FR, Dewi WK, et al. An improved method for automated calculation of the water-equivalent diameter for estimating size-specific dose in CT. *J Appl Clin Med Phys*. 2021;22(9):313-323. [Crossref]
16. Payne S, Badawy M. Comparison of average water equivalent diameter values between CTContour and vendor-specific estimates in CT dosimetry. *Phys Med*. 2023;114:103142. [Crossref]
17. Schneider CA, Rasband WS, Eliceiri KW. NIH Image to ImageJ: 25 years of image analysis. *Nat Methods*. 2012;9(7):671-675. [Crossref]
18. Sookpeng S, Martin CJ, López-González MR. Simplified approach to estimation of organ absorbed doses for patients undergoing abdomen and pelvis CT examination. *J Radiol Prot*. 2021;41(4). [Crossref]
19. Pace E, Caruana CJ, Bosmans H, Cortis K, D'Anastasi M, Valentino G. CTContour: an open-source Python pipeline for automatic contouring and calculation of mean SSDE along the abdomino-pelvic region for CT images; validation on fifteen systems. *Phys Med*. 2022;103:190-198. [Crossref]